Chapter 1

Introduction

"The total number of stars in the Universe is larger than all the grains of sand on all the beaches of the planet Earth." (Carl Sagan, Cosmos)

1.1 Motivation and Outline

Looking up to the dark night sky, the human eye is capable of identifying roughly 5000–6000 individual stars. This is only a tiny fraction of the estimated 200 billion stars in our galaxy, which again is only one out of an estimated 200 billion galaxies inhabiting our universe. Each star is shaped by the surroundings and conditions during its formation, and therefore tells a unique story. Intrinsic variability of massive stars such as Cepheid variables, for example, as well as violent explosions known as type Ia supernovae, allow us to accurately measure distances to galaxies and hence map the large-scale structure of the universe. Stars are also estimated to contain roughly $\sim 75\,\%$ of the total mass of the observable matter in galaxies (Weigert and Wendker 1989), building the primary component of the interstellar cycle of matter that makes up the structure and chemical composition of spiral galaxies like our Milky Way. Furthermore, stars are crucial to our search for Earth-like planets outside our solar-system, providing the vital clues necessary for the indirect detection of extrasolar planets and for determining the extent of the region around the host star where life can be expected to exist (the so-called habitable zone). Finally, stars are ideal laboratories to study fundamental physical processes such as energy transport through convection and to study elementary particles such as neutrinos. Evidently, the understanding of the structure and evolution of stars is at the core of many fundamental challenges in modern astrophysics.

The basic observational approach to improve our understanding of stars is to determine their fundamental properties such as mass, radius, temperature, chemical composition and age for a variety of evolutionary stages. However, constraining these fundamental properties is a challenging task. Ideally, the goal of observational stellar astrophysics is to measure these properties and compare them to predictions made using stellar models. In practice, such direct measurements are largely impossible due to the vast distances separating our solar system from even the closest stars in the solar neighbourhood. Conventional techniques to determine fundamental properties, such high-resolution spectroscopy and broadband photometry, rely heavily on the comparison with stellar models, and therefore have limited ability to improve our knowledge of stellar evolution. While direct measure-

ments of stellar masses and radii using eclipsing binary systems have been possible for a limited sample of stars, the recent era of space-based observatories operating outside the turbulent atmosphere, as well as recent technological advances improving the sensitivity of CCD-detectors, have allowed the application of two powerful observational techniques to a large number of stars. Asteroseismology, the study of stellar oscillations, enables us to accurately infer stellar properties by measuring the timescales of acoustic waves traveling through the stellar interior. Optical long-baseline interferometry achieves high resolution through the combination of light from multiple telescopes and allows us to measure the angular size of stars, which can be used to directly infer a star's physical size and temperature. The underlying main topic of this thesis is the use of both these observational techniques to study cool, low-mass (commonly referred to as solar-type) stars in different evolutionary phases to improve our understanding of their structure and evolution.

This thesis is organized as follows. The remainder of this chapter will give an introduction to the basic astrophysical concepts of stellar structure and evolution, as relevant for all later chapters. Chapter 2 introduces the basic concepts of the first main observational technique in this thesis, asteroseismology, and provides some background information on the principal instrument used in the asteroseismic analyses, the *Kepler* space telescope. Chapters 3–6 then present results from asteroseismology, both for large numbers of stars (Chapters 3–5) and for a single star of particular interest (Chapter 6). The second observational technique, long-baseline interferometry, is then introduced in Chapter 7, including a detailed description of the instrument used for interferometric studies, the PAVO beam combiner at the CHARA Array. Chapters 8–10 then present interferometric campaigns to measure fundamental properties of stars, with particular focus on the combination of these constraints with asteroseismology. Finally, Chapter 11 provides a summary of all results and a discussion of future work related to the main topics of this thesis.

1.2 Stellar Structure and Evolution

This section gives a brief introduction to the main stages of stellar evolution relevant for this thesis. The description presented here largely follows the standard works by Cox and Giuli (1968) and Kippenhahn and Weigert (1994), to which the reader is referred for more detailed information.

A traditional way to follow the evolution of stars is by plotting stellar luminosity versus effective temperature in a Hertzsprung-Russell (H-R) diagram, as shown in Figure 1.1(a) for a set of typical masses. Five critical points of stellar evolution discussed below are marked by symbols, and their luminosity can be followed as a function of stellar age in Figure 1.1(b).

1.2.1 Main Sequence

After the formation of a star through the gravitational collapse of gas in a protostellar disc, the ignition of nuclear fusion converting hydrogen into helium in the core marks the starting point of stellar evolution, often referred to as the zero-age main sequence (ZAMS, see dashed line in Figure 1.1(a)). Under the assumption of an ideal gas, fundamental properties of stars on or near the ZAMS can be approximately expressed by homology relations (Kippenhahn and Weigert 1994):

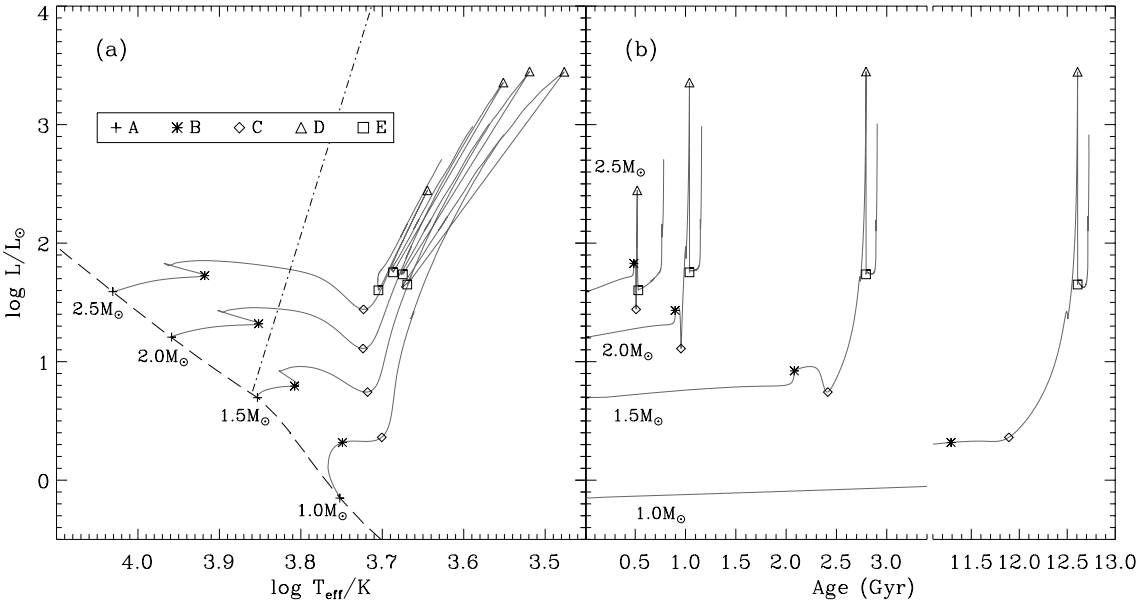

Figure 1.1: (a) Hertzsprung-Russell diagram showing BaSTI evolutionary tracks (Pietrinferni et al. 2004) for different masses and solar-scaled chemical composition (solid lines). The dashed line connects the zero-age main sequence (ZAMS), and the dashed-dotted line shows the empirical cool edge of the instability strip taken from Pamyatnykh (2000). Symbols mark five distinct points of stellar evolution along each track: A - ZAMS; B - Hydrogen exhaustion in the core; C - Bottom of the red-giant branch; D - Ignition of Helium-core burning; E - Helium-core burning main-sequence. *(b)* Same as panel (a) but plotting luminosity as a function of stellar age. Note that the abscissa is broken between 3.4 and 11.1 Gyr.

$$L \propto M^{s_1} \mu^{s_2} \tag{1.1}$$

$$R \propto M^{z_1} \mu^{z_2} \tag{1.2}$$

where L is the stellar luminosity, M is the stellar mass, R is the stellar radius, and μ is the mean molecular weight. Assuming thermodynamic equilibrium, the radius and luminosity of a star are connected to the effective temperature by the Stefan-Boltzmann law:

$$\left(\frac{T_{\rm eff}}{T_{\rm eff,\odot}}\right)^4 = \left(\frac{L}{L_\odot}\right)\left(\frac{R}{R_\odot}\right)^{-2} . \tag{1.3}$$

Assuming a constant chemical composition, Equations (1.1), (1.2) and (1.3) directly connect the fundamental parameters L, $T_{\rm eff}$ and M to form a sequence of stars for which the location on the main-sequence is primarily determined by the stellar mass. Typical observed values for such simple relations along the ZAMS are $L \propto M^{3.9}$ and $R \propto M^{0.8}$ (Kippenhahn and Weigert 1994), i.e. higher-mass stars have higher luminosities and temperatures than low-mass stars.

As a star evolves on the main-sequence (A→B in Figure 1.1), the hydrogen in the core is slowly converted into helium. This causes an increase in the mean molecular weight, which leads to an increase in luminosity (see Equation (1.1)). The exact behaviour depends on the stellar mass. Stars with $M \gtrsim 1.3\,M_\odot$ have a convective core and the dominant

energy production mechanism is the CNO cycle, in which carbon, nitrogen and oxygen isotopes are involved in nuclear reactions that create helium nuclei from hydrogen. Due to the convective core, the enhanced helium content mixes in the central regions of the star. This forms a discontinuity in μ and hence an abrupt decrease in density at the boundary to the outer radiative regions. According to the condition of hydrostatic equilibrium, a decrease in density corresponds to a decrease in the pressure gradient. Since the pressure gradient from the core to the surface must be continuous, this causes the pressure to reach zero at a larger radial distance than before, and hence the star increases in radius. At the same time, the central temperature during hydrogen burning dominated by the CNO cycle changes only slowly, and hence the increase in radius shifts the star to the right in the H-R diagram. The exhaustion of hydrogen in the core is followed by a rapid contraction of the star, which causes an increase in temperature, shifting the star to left in the H-R diagram (which can be seen as a "hook" feature in Figure 1.1(a)).

Low-mass stars like our Sun have a radiative core, and hydrogen is hence consumed gradually from the core. The mean molecular weight therefore continuously decreases towards the outer layers of the star which results in a smaller increase in stellar radius as more hydrogen is converted into helium, since no discontinuity in the pressure gradient exists. Additionally, the main energy production mechanism for these stars (the p-p chain) causes a large increase in central temperature (decrease in radius) with time, which compensates for the increase in μ. Hence, low-mass stars evolve on the main-sequence along a path almost parallel to the ZAMS, as shown in Figure 1.1(a).

Figure 1.1(b) shows that the main-sequence stage of hydrogen-core burning comprises the longest evolutionary stage for all stars. The lifetime of a star on the main-sequence is strongly dependent on stellar mass, with massive stars burning through their hydrogen much more rapidly than low mass stars. Stars with masses similar to our Sun spend roughly 11 Gyr in a stage of quiescent hydrogen-core burning, while the main-sequence lifetime of $2\,M_{\odot}$ stars is roughly ten times shorter.

1.2.2 Subgiant Phase

After hydrogen is depleted in the core of low and intermediate-mass stars, they enter a phase in which energy is provided by hydrogen burning in a shell surrounding an isothermal helium core. For higher-mass stars, the core mass increases until the pressure of the non-degenerate core can no longer support the outer layers of the star. At this point, the core contracts rapidly while the surrounding shells expand, causing a rapid increase in stellar radius accompanied by a decrease in temperature (B→C in Figure 1.1). The time scale of this process is approximately the Kelvin-Helmholtz timescale, which is very short compared to an evolutionary timescale (see Figure 1.1(b)). The chances of observing stars in this phase of evolution is therefore very small, and this causes the well-known Hertzsprung-gap in the H-R diagram.

For low-mass stars, the lower core temperature after hydrogen burning results in a higher central density and a core consisting of electron-degenerate gas, a fundamental particle density limit set by the Pauli exclusion principle of quantum mechanics. The core hence becomes supported by degeneracy pressure, and the transition from Hydrogen-core to Hydrogen-shell burning is a relatively slow and quiescent stage in evolution, taking up roughly 5% of the main-sequence lifetime for stars with a mass similar to the Sun. Stars observed in this region of the H-R diagram are commonly referred to as subgiant stars.

1.2.3 Red Giant Branch to Red Clump

As the temperature in the envelope decreases during the contraction of the helium core, the surface convection zone becomes deeper until the star approaches the so-called Hayashi line, a theoretical limit for fully convective stars. At this point hydrogen-shell burning continues with a slowly decreasing temperature. Since the core mass mainly determines the luminosity of a star, the increasing core mass due to hydrogen-shell burning increases the luminosity and the star moves up the so-called red giant branch (RGB; C→D in Figure 1.1). Stars ascending the red giant branch have very similar effective temperatures regardless of mass, ranging from approximately 3000 to 5500 K. At the same time the radii of stars increase dramatically, reaching up to 200 times the values on the main sequence.

The further evolution is again dependent on stellar mass. For high-mass stars ($M \gtrsim 2M_\odot$), core contraction continues until the central temperature is high enough for helium to ignite in the core. This occurs at the tip of the red-giant branch (TRGB; point D in Figure 1.1). The critical core mass at the TRGB is a function of stellar mass, with higher-mass stars igniting helium at lower luminosities. Meanwhile, stars with $M \lesssim 2M_\odot$ ignite helium in an electron-degenerate core. In these conditions, the critical core mass for helium ignition occurs at a value of $M_c \sim 0.45\,M_\odot$, independent of stellar mass. The TRGB therefore occurs at a roughly constant luminosity. The helium ignition in degenerate matter is unstable and leads to a thermal runaway, the so-called helium flash. The threshold mass $M_{\rm He}$ dividing these two scenarios of helium-ignition is considered a sensitive probe for determining details about convection (see Section 1.2.4).

After helium ignition, core contraction stops. The core starts to expand and the envelope shrinks, causing a rapid decrease in luminosity (D→E in Figure 1.1). Stars settle in a relatively long-lived, stable phase of burning helium in the core, with hydrogen-burning continuing in a surrounding shell. For low-mass stars, this stage takes up roughly 1% of the main-sequence lifetime and is referred to as the helium-core burning main-sequence or horizontal branch. Since all stars below the threshold mass $M_{\rm He}$ ignite helium at a similar core-mass, their luminosities after the helium flash are very similar. We hence find many stars in this region of the H-R diagram, and this characteristic feature is referred to as the red clump. Stars with masses above the threshold also settle on the helium-core burning main sequence, but have slightly lower luminosities. They form a second population, commonly referred to as the secondary clump (Girardi 1999).

1.2.4 Chemical Composition and Convection

Several effects can complicate the relatively simple picture of stellar evolution described in the previous sections. The main-sequence M-R and M-L relations depend on the mean molecular weight μ and opacity κ, which can be altered by different initial chemical compositions. The chemical composition is usually expressed as the mass fractions of hydrogen (X), helium (Y) and all elements heavier than helium (Z), so that $X+Y+Z=1$. For the Sun, typical adopted values are $Y = 0.27$ and $Z = 0.02$, making it metal-rich compared to the average metallicity in the solar-neighbourhood (Nordström et al. 2004).

Figure 1.2(a) shows the effect of changing the initial chemical composition for a $1.5\,M_\odot$ model. As the amount of heavy elements increases, the opacity increases, causing the tracks to move to lower luminosity and lower temperature (see Equations (1.1) and (1.2)). Metal-poor stars therefore appear hotter and more luminous than stars with the same mass

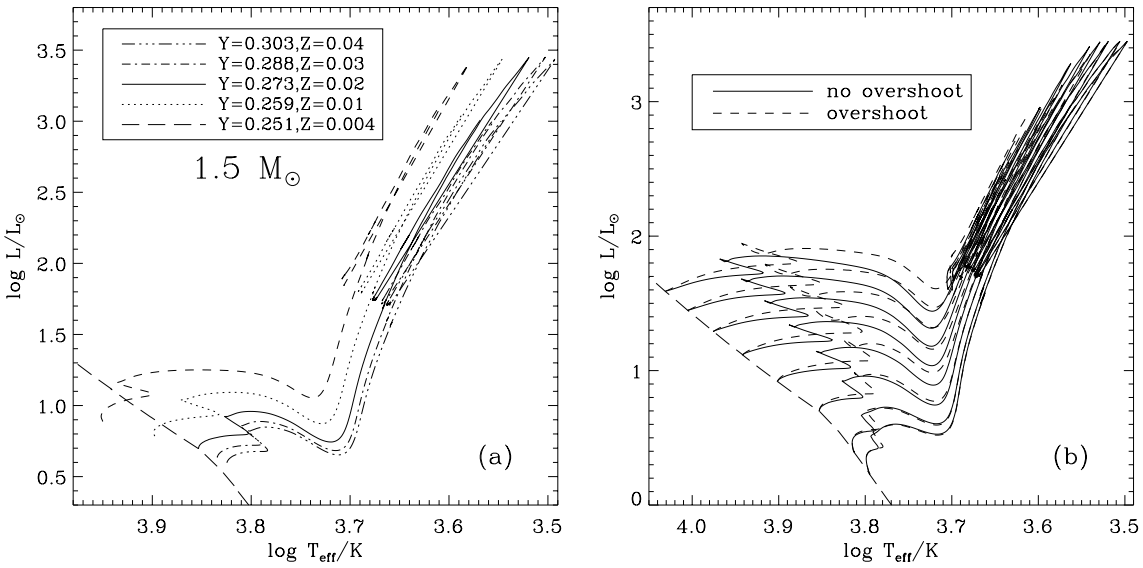

Figure 1.2: (a) Hertzsprung-Russell diagram showing BaSTI evolutionary tracks (Pietrinferni et al. 2004) for a 1.5 $M_{\odot}$ model with different initial chemical compositions. *(b)* Evolutionary tracks for solar metallicity and $M = 1.3 - 2.5\,M_{\odot}$ in steps of $0.2\,M_{\odot}$for models with and without convective core overshooting. The long-dashed line marks the zero-age main sequence (ZAMS) for solar metallicity in both panels.

and higher metallicity. As evident from this discussion, the accurate determination of the fundamental properties of stars, in particular age, are heavily dependent on constraints of stellar metallicity, which can usually be acquired by modeling high-resolution spectra.

A more serious uncertainty in calculating stellar models is the treatment of convection. In the absence of proper analytical models, convection is commonly described by models in which the convection efficiency (or more accurately, the distance over which a convection element mixes with it surroundings) is treated as a free parameter. Such theories include the standard mixing-length theory of convection, with $\alpha_{\rm MLT}$ as the mixing-length parameter. More efficient convection is described by a larger value of $\alpha_{\rm MLT}$ and results in a hotter effective temperature for a star with a given R, M and chemical composition. Another important parameter is the convective core overshooting parameter $\alpha_{\rm OV}$, describing the physical distance over which convective cells exist beyond the standard convection stability (Schwarzschild) criterion. Figure 1.2(b) shows the effect of including overshooting in stellar models of various masses and fixed chemical composition. The general effect of overshooting is to prolong the main-sequence lifetime, since an extra supply of hydrogen is provided by the larger convective core, causing the "hook" to move to lower temperatures. The amount of convective overshooting is modeled as a function of stellar mass, which can be seen by the decreasing temperature of the hook as the stellar mass decreases.

This short description of physical effects influencing stellar evolution illustrates the need for dedicated observational campaigns to determine fundamental properties of stars in different stages of evolution. Accurate masses, radii and temperatures can be used to put tight constraints on theories determining opacities of radiative transfer and the treatment of convection, which are needed to advance our physical understanding of these processes. To do this, observational techniques to directly measure fundamental stellar properties, such as asteroseismology and interferometry, are required.

Chapter 2

Asteroseismology of Cool Stars

One of the most powerful tools to study the interior structure and fundamental properties of stars is asteroseismology, the study of the intrinsic variability due to stellar pulsations. The periodic contraction and expansion of gas in a star enables us to probe the structure of the stellar interior, since the timescales of the variations are directly related to the physical properties (such as density and temperature) of the gas itself. An illustrative analogy can be made by comparing pulsating stars with musical instruments: the frequency of the sound that is perceived by the human ear is directly related to the size and material of the instrument, with larger instruments (such as a tuba) sounding in lower tones than smaller instruments (such as a flute)[1].

The following section gives a basic introduction to asteroseismology of cool stars following largely the works by Christensen-Dalsgaard (2003) and Aerts et al. (2010), to which the reader is referred for more detailed information. Regarding asteroseismology in hotter stars (such as δ Scuti stars, slowly pulsating B stars, and compact pulsators), the interested reader is referred to Breger (2000), Balona (2009), Fontaine and Brassard (2008) and references therein. The second part of this chapter will then provide some background information on the *Kepler* space telescope, the main instrument used in the asteroseismic studies presented in the following chapters.

2.1 Introduction to Asteroseismology

2.1.1 Fundamentals

An oscillation mode in a spherical symmetric object can be described using spherical harmonics, as follows:

$$Y_l^m(\Theta, \Phi) = (-1)^m \, c_{lm} \, P_l^m \, \cos(\Theta) \, e^{(im\Phi)} \, . \tag{2.1}$$

Here, Θ and Φ are the co-latitude (latitude measured from the pole) and longitude in the spherical coordinate system, $P_l^m \cos(\Theta)$ are Legendre polynomials and c_{lm} a normalization constant so that the integral of the left hand side of Equation 2.1 over the unit sphere is 1. Each spherical harmonic is characterized by the quantum numbers l and m. The spherical degree l corresponds to the total number of node lines on the surface. The azimuthal

[1] For an interesting example of taking this analogy to a whole different level, the reader is referred to the appendix of this thesis.

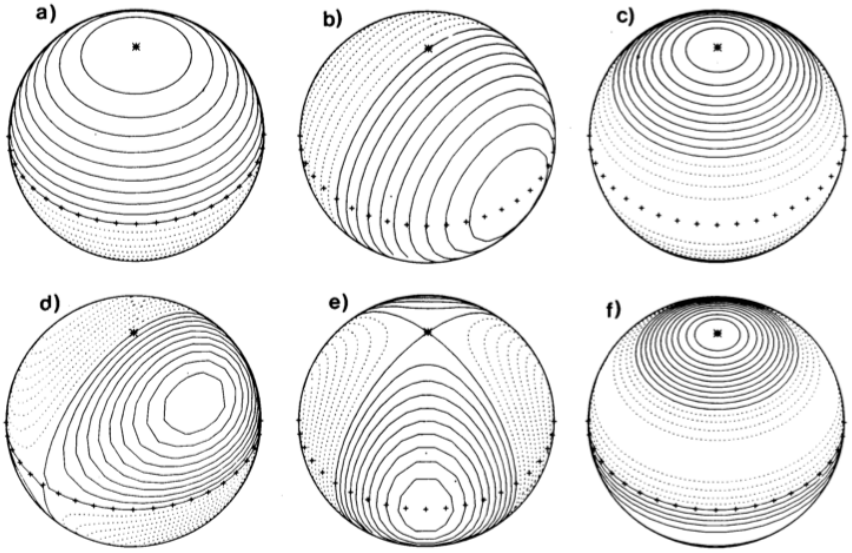

Figure 2.1: Real part of the spherical harmonics Y_l^m. Solid lines show parts of the star moving towards the observer, dotted lines parts that move away. The pole of the star is indicated by star-signs, the equator by plus-signs. The following cases are shown: a) $l = 1$, $m = 0$; b) $l = 1$, $m = 1$; c) $l = 2$, $m = 0$; d) $l = 2$, $m = 1$; e) $l = 2$, $m = 2$; f) $l = 3$, $m = 0$. From Christensen-Dalsgaard (2003).

order is expressed by m, and $|m|$ denotes the number of node lines in the longitudinal direction. The azimuthal order takes values ranging from $-l$ to l (so that $2l + 1$ modes for each degree l), and is important for rotating stars for which the degeneracy imposed by spherical symmetry is broken. The special case of radial pulsations is expressed as $l = 0$, and corresponds to the star expanding and contracting as a whole (sometimes also called the "breathing mode"). Spherical degrees greater than zero are hence referred to as non-radial pulsations, with $l = 1$ being dipole, $l = 2$ quadrupole and $l = 3$ octupole modes. Figure 2.1 shows some examples of solutions to Equation (2.1) for several configurations of l and m. Note that since stars are usually observed as point sources (i.e. they are not spatially resolved), cancellation effects generally prevent the observation of high degree ($l > 3$) modes. In addition to l and m, oscillation modes are further characterized by the radial order n, the number of nodes along a radius from the surface to the center of the star.

In general, we discern between two main types of pulsation modes in stars: pressure modes (p modes) and gravity modes (g modes). p modes are acoustic waves propagating through the stellar interior by the compression and decompression of gas, and the pressure gradient acts as the restoring force. g modes correspond to modes in which gas is oscillating due to buoyancy and gravity, and buoyancy acts the restoring force. Note that for g modes, no radial ($l = 0$) modes exist and the radial order n is conventionally counted as negative.

The main properties of p modes and g modes can be illustrated using a so-called propagation diagram, as shown in Figure 2.2. This diagram shows the characteristic oscillation frequency for p modes (Lamb frequency, dashed lines) for different values of l as well as for g modes (Brunt-Väisälä frequency, solid line) as a function of stellar radius for a model of the Sun. Pressure modes with lower spherical degree propagate deeper into

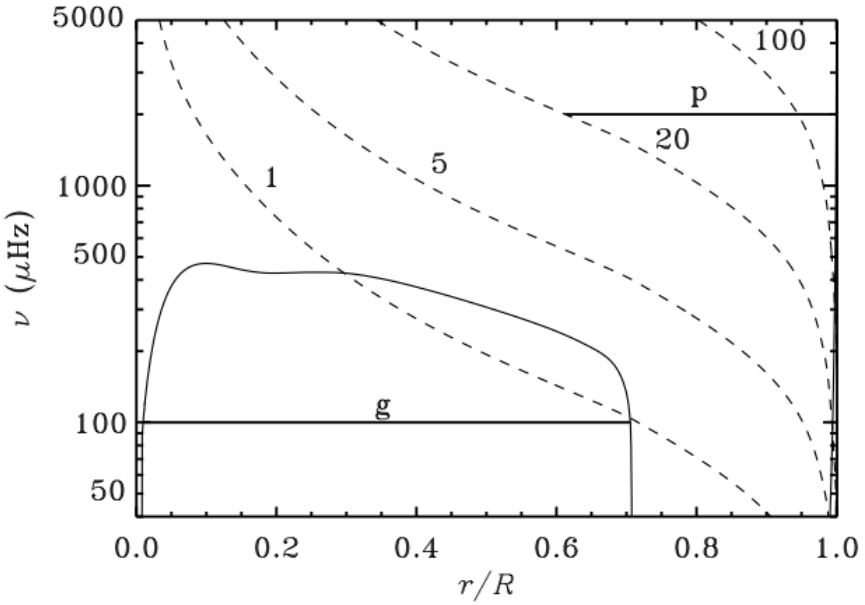

Figure 2.2: Propagation diagram of oscillation modes for a model of the Sun. Dashed lines mark the characteristic p-mode frequencies for modes of different degree l. The solid line marks the characteristic g-mode frequency. Thick horizontal solid lines show the trapping region of a g mode with a frequency of $100\,\mu$Hz and a $l = 20$ p mode with a frequency of $2000\,\mu$Hz. From Christensen-Dalsgaard (2003).

the star than modes with higher l. The reflection of non-radial modes at the inner turning point is caused by the change in sound speed as the density increases towards the stellar interior. g modes, on the other hand, have lower frequencies and are confined to the deep interior of the star where convection is stable. g modes are therefore trapped in the stellar interior, making their detection extremely difficult. For stars like our Sun, in which p modes are excited at frequencies around $3000\,\mu$Hz, the p-mode and g-mode cavities are well separated, and the amplitudes of g modes on the surface are very small. More evolved stars such as subgiants and red giants oscillate at lower frequencies and oscillation modes can have a mixed character, being p modes at the surface and g modes in the center. Such mixed-modes have a particularly high diagnostic potential for inferring properties about the interior of stars (see, e.g., Bedding et al. 2011).

2.1.2 Excitation Mechanisms

What causes stellar pulsations? There are two main excitation mechanisms. For massive stars ($M \gtrsim 2M_{\odot}$), pulsations are driven by temperature-dependent opacity changes in certain layers of the star, causing radiation pressure to continuously expand a star past its equilibrium point before contracting again under the force of gravity. This heat-engine mechanism (also called κ mechanism) causes a coherent driving of modes which lasts over long timescales of stellar evolution. The κ mechanism acting in the helium ionization zone is effective in a region of the H-R diagram referred to as the classical instability strip, including pulsators such as δ Scuti, γ Doradus and RR-Lyrae stars, as well as Cepheid variables. The dashed line in Figure 1.1 shows the empirically determined cool edge of the

instability strip from observations of δ Scuti stars by Pamyatnykh (2000).

Oscillations in cooler, low-mass stars like our Sun are caused by the turbulent motions of gas due to convection in the outer layers of the star. The acoustic energy in the convective zone excites oscillation modes stochastically, and hence their lifetimes in our Sun are typically only a few days. Oscillations of this type are commonly referred to as solar-like oscillations, although they are also found in more evolved stars with convective envelopes such as red giants. The exact mechanism of the driving and damping of these modes and the transition to higher-mass stars oscillating due to the κ mechanism is still relatively poorly understood, owing largely to our restricted understanding of stellar convection (see, e.g., Houdek et al. 1999; Houdek 2006; Dupret et al. 2005).

2.1.3 Properties of Solar-like Oscillations

Oscillation frequencies $\nu_{n,l}$ of high radial order n and low spherical degree l can be described by the so-called asymptotic theory of stellar oscillations (Tassoul 1980; Gough 1986), as follows:

$$\nu_{n,l} = \Delta\nu(n + \frac{1}{2}l + \epsilon) - \delta\nu_{0l} \, . \tag{2.2}$$

Equation (2.2) predicts that oscillation frequencies follow a series of characteristic spacings. The large frequency separation $\Delta\nu$ is the separation of modes of the same spherical degree l and consecutive radial order n. Furthermore, modes of the different degree l and same radial order n are expected to be separated by the small frequency separations $\delta\nu_{0l}$, which are defined as follows:

$$\delta\nu_{02} = \nu_{n,0} - \nu_{n-1,2} \, , \tag{2.3}$$

$$\delta\nu_{01} = \frac{1}{2}(\nu_{n,0} + \nu_{n+1,0}) - \nu_{n,1} \, , \tag{2.4}$$

$$\delta\nu_{13} = \nu_{n,1} - \nu_{n-1,3} \, . \tag{2.5}$$

Figure 2.3 shows a power spectrum of observations of the Sun, illustrating the regular spacings of peaks with different degree l and n, as well as the large and small frequency separations. It can be seen that the individual peaks are slightly broadened, which is a signature of the finite lifetime of the modes (see previous section). The mode lifetime τ is related to the full-width half-maximum Γ of the Lorentzian envelope as:

$$\tau = \frac{1}{\Gamma\pi} \, . \tag{2.6}$$

For the Sun typical observed linewidths are $1 - 2\,\mu$Hz, corresponding to mode lifetimes of 2–4 days.

A common tool to analyze the regular spacings of solar-like oscillations is the so-called échelle diagram (Grec et al. 1983), in which all frequencies are plotted modulo the large frequency separation (see Figure 2.4). By doing this, all modes of the same degree l line up as nearly-vertical ridges, with ridges of different degree separated by the small spacings as given in Equations (2.3)–(2.5). The constant ϵ in Equation (2.2) is related to the inner and outer turning point of the oscillations, and therefore depends on the properties of the surface layers of the star. For a given $\Delta\nu$, it can be determined by measuring the offset

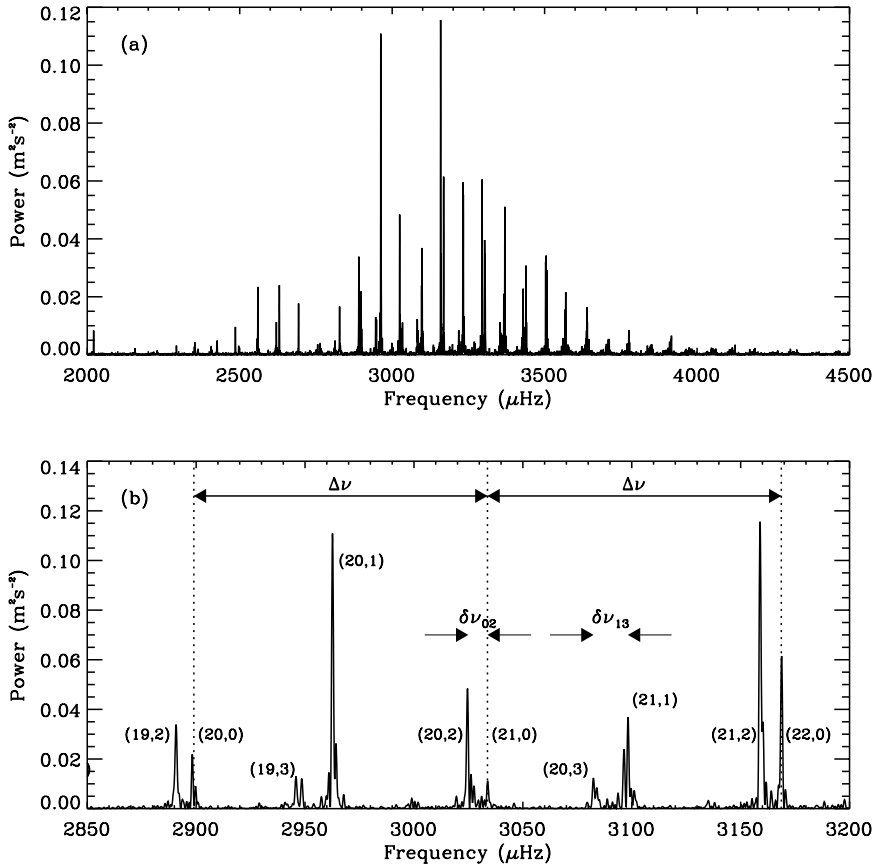

Figure 2.3: (a) Power spectrum of 10 days of velocity observations of the Sun taken with the BiSON instrument (Chaplin et al. 1997b). *(b)* Close-up of panel (a) near the frequency of maximum power, indicating the spherical degree l and radial order n for each mode. Dotted lines mark the radial modes, and the large and small separations are indicated. From Bedding (2011).

of the $l = 0$ ridge in the échelle diagram, as shown in Figure 2.4. Since the radial order n is usually not known, the value of ϵ is ambiguous by ± 1 (see Equation (2.2)). For the Sun, theoretical models show that $\epsilon \sim 1.5$. Also, it is important to note that $\Delta\nu$ and ϵ are highly correlated, since a change in $\Delta\nu$ will slightly shift the ridges across the échelle diagram (see, e.g., White et al. 2011).

Physically, the large and small frequency separations are very useful since they depend on the internal sound speed profile of the star. In the asymptotic theory, the large frequency separation can be shown to be the inverse of twice the sound travel time from the surface to the center (Christensen-Dalsgaard 2003):

$$\Delta\nu = \left(2\int_0^R \frac{dr}{c}\right)^{-1} , \tag{2.7}$$

where the sound speed c, assuming adiabacity, is given by

$$c = \sqrt{\Gamma_1 p/\rho}\,. \tag{2.8}$$

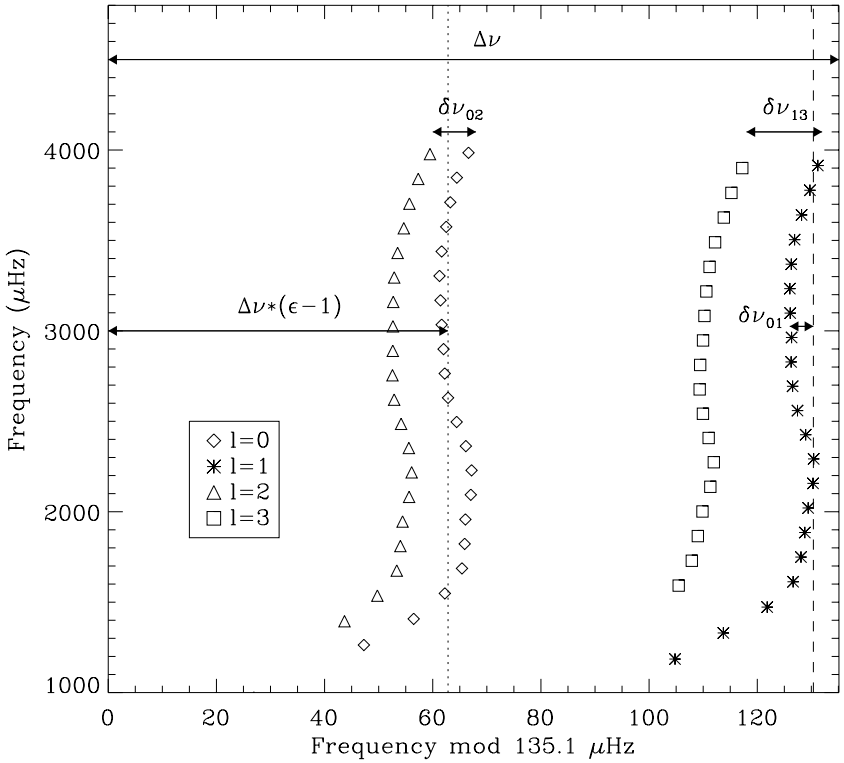

Figure 2.4: Échelle diagram of detected oscillation modes in the Sun (Broomhall et al. 2009). The dotted line marks the approximate centroid of the $l = 0$ ridge to illustrate the measurement of ϵ. The dashed line marks the midpoint between $l = 0$ modes based on the centroid shown by the dotted line. The large and small separations are also marked.

Here, Γ_1 is an adiabatic exponent, p is the pressure and ρ is the density. For an ideal gas, we have $\rho \propto \mu P/T$ (Kippenhahn and Weigert 1994) and therefore

$$c \propto \sqrt{T/\mu}\,. \tag{2.9}$$

The sound speed therefore depends on the average internal temperature and chemical composition of the gas. For an ideal gas, basic estimates for the central temperature give $T \propto \mu M/R$ (Kippenhahn and Weigert 1994), and hence

$$\Delta\nu \propto \left(\frac{M}{R^3}\right)^{1/2}\,. \tag{2.10}$$

The large frequency separation is therefore a direct measure of the mean density of a star. In practice, Equation (2.10) has been shown to be accurate to a few percent (Stello et al. 2009a; White et al. 2011). As can be seen in Figure 2.4, the mode ridges are curved, indicating that the asymptotic relation in Equation (2.2) is only an approximation. The curvature of mode ridges can be described as a variation of $\Delta\nu$ with frequency, and probes the internal structure of the star such as the base of the convection zone (Christensen-Dalsgaard 2003). Note that Bedding (2011) has suggested that it is physically more

sensible to describe the curvature as a variation of ϵ with frequency.

The small frequency separations can be written as:

$$\delta\nu_{nl} = -(4l+6)\frac{\Delta\nu}{4\pi^2\nu_{nl}}\int_0^R \frac{dc}{dr}\frac{dr}{r}\,. \tag{2.11}$$

The integral shows that $\delta\nu_{nl}$ is sensitive to sound-speed gradient in the stellar interior which, as shown in Equation (2.9), is itself dependent on the chemical composition profile. Hence, $\delta\nu_{nl}$ is sensitive to changes in the chemical composition during stellar evolution (see Section 1.2) and thus to the stellar age. Equation (2.11) can be qualitatively understood by the fact that modes of different spherical degree l travel to different depths within the star (see Figure 2.2), and hence their frequency differences provide information about the radial structure. As can be seen in Figure 2.4, the small frequency separations vary as a function of frequency and spherical degree l, as predicted by Equation (2.11). Again this can be qualitatively understood by recalling that the depth to which modes penetrate the star depends not only on l but also on the frequency of the mode (see Figure 2.2).

Apart from frequency separations, there are two other important observables for solar-like oscillations. Figure 2.3 shows that the power excess of oscillation has a roughly Gaussian shape, reaching a maximum at a certain frequency. This maximum defines the frequency of maximum power ($\nu_{\rm max}$) as well as the maximum amplitude of the oscillation, both of which are related to the driving and damping of the modes. The frequency of maximum power has been suggested to scale with the acoustic cut-off frequency (Brown et al. 1991), which is the maximum frequency below which an acoustic mode can be reflected (Christensen-Dalsgaard 2003):

$$\nu_{\rm ac} = \frac{c}{2H_{\rm p}}\,. \tag{2.12}$$

Here, $H_{\rm p}$ is the pressure scale height which, for an isothermal atmosphere, is given by (Kippenhahn and Weigert 1994):

$$H_{\rm p} = \frac{PR^2}{GM\rho}\,. \tag{2.13}$$

Using the same approximation as above for an ideal gas and assuming that the temperature can be approximated by the effective temperature $T_{\rm eff}$, we have:

$$\nu_{\rm max} \propto \nu_{\rm ac} \propto \frac{M}{R^2\sqrt{T_{\rm eff}}}\,. \tag{2.14}$$

$\nu_{\rm max}$ is therefore primarily sensitive to the size of the star and hence a good indicator of the evolutionary state. Typical oscillation periods range from a few days to weeks for red-giant stars to a few minutes for main-sequence stars like our Sun.

Finally, based on models by Christensen-Dalsgaard and Frandsen (1983), Kjeldsen and Bedding (1995) have suggested that amplitudes of solar-like oscillations observed in velocity scale as:

$$v_{\rm osc} \propto \left(\frac{L}{M}\right)^s\,. \tag{2.15}$$

Kjeldsen and Bedding (1995) also argued that the oscillation amplitude A_λ observed in photometry at a wavelength λ is related to the velocity amplitude as follows:

$$A_\lambda \propto \frac{v_{\rm osc}}{\lambda} T_{\rm eff}^{-r} \ . \tag{2.16}$$

Lacking a precise theory for convection, which is responsible for the driving and damping of the modes, the coefficients s and r are generally not well-constrained by theory. An in-depth investigation of the scaling law for amplitudes including estimates for these coefficients from observations will be presented in Chapter 5.

The global parameters $\Delta\nu$, $\delta\nu_{nl}$, $\nu_{\rm max}$, ϵ and A form the main set of observables in any asteroseismic analysis of solar-like oscillations. They are the main focus of the investigations presented in Chapters 4–6.

2.1.4 Observations of Solar-like Oscillations

The following section provides a brief introduction to the techniques and history of observations of solar-like oscillations. It by no means does justice to all the major efforts that have gone into the observations of oscillations in the past two decades, and I refer the reader to the review articles by Brown and Gilliland (1994), Bedding and Kjeldsen (2003), Christensen-Dalsgaard (2004), Aerts et al. (2008) and Bedding (2011) for additional details and references.

Stellar oscillations involve a physical expansion and contraction of stars and therefore cause variations in stellar brightness. Monitoring the stellar brightness can therefore be used to determine the oscillation frequencies of a star. An alternative method is to measure the wavelength shift of spectral lines due to the Doppler effect. Depending on the chosen spectral line, velocity measurements are sensitive to slightly different layers of the star compared to luminosity variations which mostly probe photospheric variations. Observations in intensity depend on temperature changes and are therefore more sensitive to stochastic noise caused by stellar granulation, which can complicate the detection of solar-like oscillations. Velocity measurements, on the other hand, are also more sensitive to detecting higher angular degree modes. The power spectrum of velocity measurements shown in Figure 2.3, for example, shows the clear signature of $l = 4$ modes (e.g. at $\sim 3000\,\mu$Hz), which are generally undetectable in luminosity measurements. A third method to detect oscillations is based on measuring the equivalent widths of spectral lines, which are sensitive to temperature (and therefore luminosity) fluctuations (Kjeldsen et al. 1995; Bedding et al. 1996).

Early detections of solar-like oscillations mostly relied on spectroscopic observations, since atmospheric scintillation in most cases prevents ground-based photometry from reaching the precision required to detect solar-like oscillations. The first confirmed detection of oscillations in another star than the Sun dates back to Brown et al. (1991), who reported a power excess in Procyon, followed by the first detection of regularly spaced frequencies in η Boo by Kjeldsen et al. (1995). Driven by the goal of detecting extrasolar planets using Doppler shifts, the sensitivity of velocity measurements greatly improved and enabled the detection of oscillations in several nearby main-sequence and subgiant stars such as β Hyi (Bedding et al. 2001; Carrier et al. 2001), α Cen A (Bouchy and Carrier 2001; Butler et al. 2004) and B (Carrier and Bourban 2003; Kjeldsen et al. 2005) as well as red giant stars such as ξ Hya (Frandsen et al. 2002) and ϵ Oph (De Ridder et al. 2006). Thanks to the larger amplitudes in red giants, detections in these stars were also possible using photometric ground-based observations (Stello et al. 2007a). In total, ground-based

efforts have yielded detections in ~ 20 stars to this date (see, e.g., Kjeldsen and Bedding 2004; Bedding and Kjeldsen 2008).

A major disadvantage of ground-based campaigns is the inability to observe stars continuously. Gaps in the time series introduce serious difficulties in extracting correct frequencies due to aliasing. This problem can be alleviated by using multi-site campaigns, which so far has only been truly realized for observations of Procyon (see Arentoft et al. 2008; Bedding et al. 2010b and Chapter 6) and M67 (Gilliland et al. 1993; Stello et al. 2007a), while dedicated networks for asteroseismology such as SONG (Stellar Observations Network Group, Grundahl et al. 2006) are currently being built. Another solution is to perform observations from space, which also removes the problem of atmospheric scintillation. The first successful mission dedicated to asteroseismology is the Canadian space telescope MOST (Microvariability and Oscillations in Stars, Walker et al. 2003; Matthews 2007), which detected solar-like oscillations in several red-giant stars (Barban et al. 2007; Kallinger et al. 2008b), as well as Procyon (see Chapter 6). Observations of solar-like oscillations from space have also been performed using the star-tracker of the WIRE (Wide-Field Infrared Explorer) satellite (Schou and Buzasi 2001; Retter et al. 2003; Bruntt et al. 2005; Stello et al. 2008), as well as the SMEI (Solar Mass Ejection Imager) experiment (Tarrant et al. 2007) and the Hubble Space Telescope (Edmonds and Gilliland 1996; Gilliland 2008; Stello and Gilliland 2009; Gilliland et al. 2011). A major breakthrough in observational asteroseismology has been achieved by the French-led CoRoT (Convection Rotation and Planetary Transits) satellite launched launched in 2006, which detected oscillations in a number of main-sequence stars (see, e.g., Michel et al. 2008) and in several thousands of red-giant stars (see, e.g., De Ridder et al. 2009; Hekker et al. 2009). Finally, the launch of the *Kepler* space telescope in 2009 has revolutionized observational asteroseismology, with thousands of detections across the cool part of the H-R diagram. A major part of this thesis is based on *Kepler* observations and will be presented in Chapters 4 and 5. The next section gives a more detailed description of the *Kepler* mission.

2.2 The *Kepler* Space Telescope

2.2.1 Motivation and Background

Finding evidence for life outside our solar system is one of the most fascinating challenges in the history of mankind. Many scientists believe that an unambiguous detection of extraterrestrial life would have profound influences on our society, and it is probably appropriate to refer to such a discovery as one of the "holy grails" of astronomy.

The reflected light of planets is tiny compared to the brightness of stars, which makes the direct detection of extrasolar planets very difficult. The first indirect detection of a planet around a main-sequence star was made in 1995 (Mayor and Queloz 1995), using the Doppler shift to detect the gravitational pull on the star 51 Peg caused by an unseen planet. The Doppler technique quickly gained popularity and revealed hundreds of extrasolar planets within a decade. However, observational bias caused the discoveries to be dominated by planets which are very much unlike Earth, being both massive and in close-in orbits (so-called Hot Jupiters). Indeed, it is now clear that the detection of an Earth-like planet in a ~ 1 year orbit around a Sun-like star using the Doppler technique will be extremely difficult because the signal caused by such a planet ($\sim 0.1\,\mathrm{m\,s^{-1}}$) is on the same order as the intrinsic variability of the star itself.

Another indirect technique, called the transit method, offers a solution to this problem. In analogy to the eclipse of the Sun by the moon or the inner planets, an extrasolar planet passing in front of the line of sight of the observer will cause a dip in brightness of the star, revealing the presence of a planet. After the first transiting exoplanet was detected by Charbonneau et al. (2000), several ground-based networks such as WASP (Pollacco et al. 2006), HATnet (Bakos et al. 2004), XO (McCullough et al. 2005) and TrES (Alonso et al. 2004) have been set up to continuously monitor the brightness of stars in the hunt for more planets. However, several factors severely limit a ground-based search for transits. Firstly, observations have to be performed as continuously as possible in order not to miss any transit events, preferably monitoring a large number of stars to increase the probability of detecting a transit. Secondly, the photometric precision must be high in order to be able to detect the signal. A Jupiter transit in front of the Sun causes a 1% dip, but an Earth-like planet causes a dip of only 0.01%, a precision which is unachievable from the ground due to atmospheric scintillation. Hence, the ideal instrument to search for transits of extrasolar planets would deliver continuous, long, high-precision photometry for a large number of stars. Such observations are also ideally suited for asteroseismology.

The idea to use a space telescope to search for photometric transits of exoplanets dates back to Rosenblatt (1971) and Borucki and Summers (1984). The first space telescope partially dedicated to search for exoplanet transits, the French-led CoRoT satellite (Baglin et al. 2009), was launched in December 2006. CoRoT has detected 18 confirmed exoplanets at the time of writing of this thesis (Hébrard et al. 2011; Deleuil et al. 2011), including the first transiting super Earth (Léger et al. 2009). Driven by the ground-based detection of exoplanets in the 1990's, the *Kepler* space telescope (named after German astronomer Johannes Kepler) was selected in 2001 as the 10th NASA discovery mission, the first one dedicated to search for Earth-like planets around stars like our Sun.

2.2.2 Design and Orbit

The left panel of Figure 2.5 shows the *Kepler* spacecraft before launch. The primary component is a modified Schmidt telescope consisting of a 0.95 m corrector lens and a 1.4 m primary mirror. The detector is located at the primary focus and consists of an array of 42 back-illuminated CCDs, each having 2200×1024 pixels with a pixel size of $27 \times 27 \mu$m. The field of view of *Kepler* is roughly 10×10 degrees in size and the plate scale is 4 arcseconds per pixel. *Kepler* observations are optimized for high photometric precision and stability. Cooling of the detectors is achieved using heat pipes connected to an external radiator located on the opposite side to the solar panels (see Figure 2.5). *Kepler* observations are performed through a custom broadband filter with a spectral bandpass from $\sim 400 - 850$ nm.

The *Kepler* space telescope was launched on March 7 2009 aboard a Delta II rocket from Cape Canaveral Air Force Station, Florida. *Kepler* was launched in an Earth-trailing, heliocentric orbit with an approximate orbital period of 373 days (see Figure 2.5). In order to optimize the efficiency of detecting planetary transits, *Kepler* was designed to monitor a fixed patch in the sky for its entire mission lifetime (nominal duration of 3.5 years, but possibly extended for another 2–6 years). This is achieved by observing a field out of the ecliptic plane while rotating the spacecraft by 90° every four months in order to keep the solar panels directed towards the Sun. The *Kepler* field of view is centered on RA = 19h 22m 40s and Dec = $+44° 30'$ towards the galactic plane in the constellations

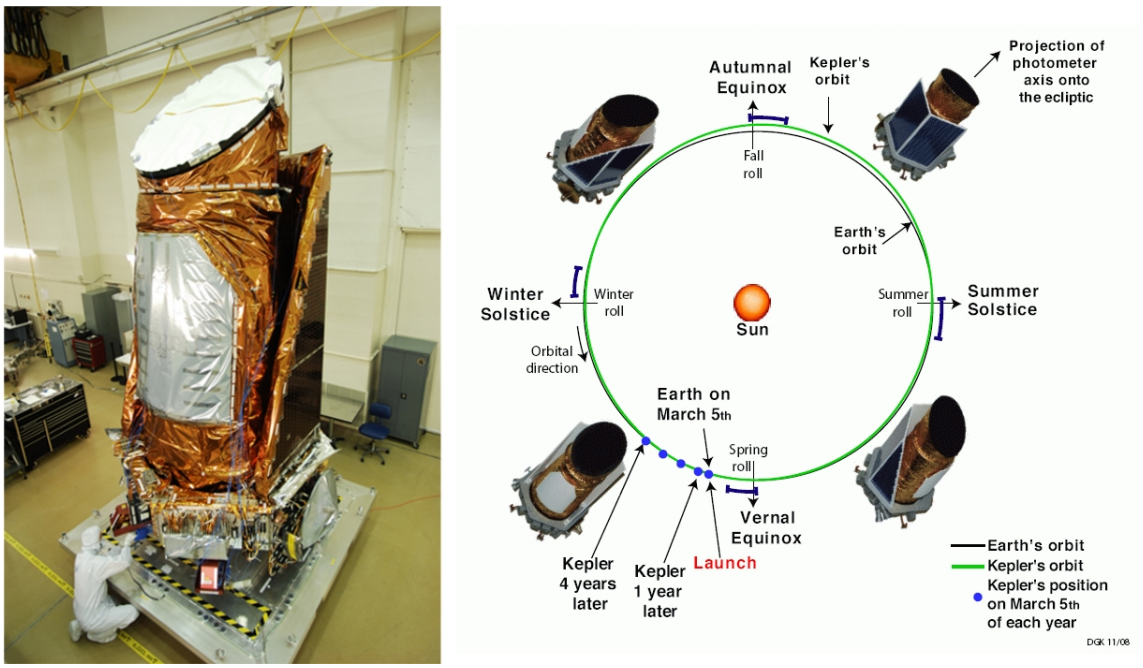

Figure 2.5: Left: The *Kepler* space telescope at Ball Aerospace laboratories where the spacecraft was built and assembled. *Right:* Schematic view of the heliocentric orbit of *Kepler* around the Sun, indicating the times of the quarterly spacecraft rolls. Image Credit: Ball Aerospace and NASA Ames.

of Cygnus and Lyra, corresponding to a line of sight along the Orion arm of our Milky Way galaxy (see Figure 2.6). *Kepler* simultaneously monitors the brightnesses of roughly 150 000 stars of spectral types F-K in a magnitude range down to $V \sim 16$, consisting mainly of main-sequence stars. *Kepler* employs two observing modes, recording data in 30-minute intervals (long-cadence mode, see Jenkins et al. 2010a) and in 1-minute intervals (short-cadence mode, see Gilliland et al. 2010b). Long-cadence data are used for the majority of the stars, while a smaller number of stars (limited by the downlink rate from the spacecraft to Earth) are observed in short-cadence mode.

2.2.3 Mission Objectives

Kepler is a statistical mission, with the primary objective of determining the frequency of terrestrial planets around stars similar to our Sun. Using the detected transits, the goal is to measure the orbital periods and radii of planets and study their distribution to infer the frequency of Earth-like planets in the so-called habitable zone (the region around a star in which liquid water can exist). Additionally, the detections are used to determine the frequency of multiple planetary systems. For a limited number of close-in planets, it is expected that secondary transits (the occultation of the reflected light of the planet as it passes behind the star) can be measured, giving information about the planet albedo and atmospheric composition. For planets bright enough to be followed up using Doppler spectroscopy, the planetary mass can be inferred. In combination with the planet radius from the transit, this gives a measure of the planetary density.

A crucial point common to almost all the mission goals is that the transit only gives

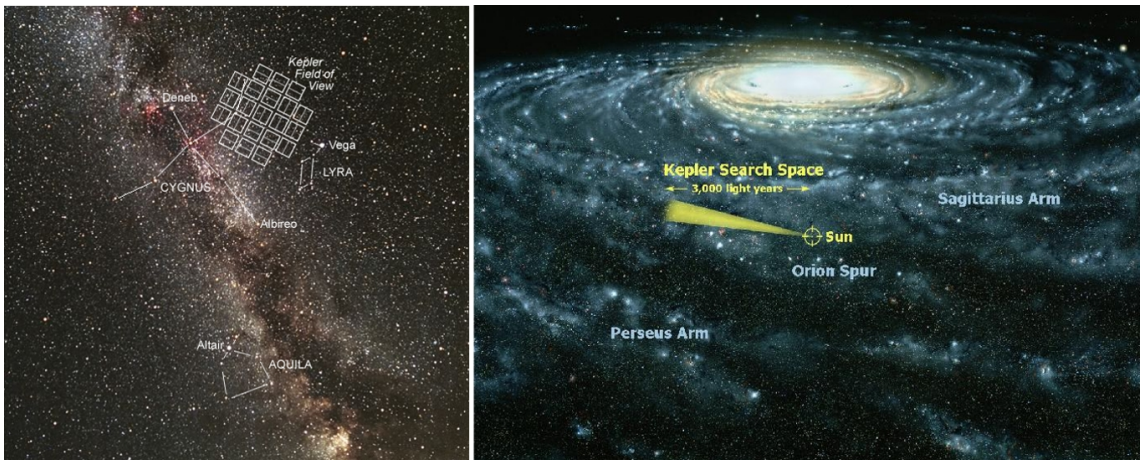

Figure 2.6: Left: Field of view of the *Kepler* space telescope projected onto the night sky. Each rectangle marks one of the 42 CCD detectors. The constellations Cygnus, Lyra and Aquila (the primary stars of which form the well-known "summer triangle" in the northern hemisphere) are also shown. *Right:* Artists impression of the Milky Way galaxy, indicating the position of our solar system and the search space covered by observations with *Kepler*. Note that the distance marked corresponds to the magnitude range of observed main-sequence stars. Image Credit: Carter Roberts and Jon Lomberg.

the size of the planet relative to the size of the star. Hence, in order to accurately constrain the radius and density of a detected planet, the radius of the host star must be accurately known. Additionally, the extent of the habitable zone around a star is determined by the stellar effective temperature and luminosity: for cool, low-luminosity stars of spectral type K, the habitable zone lies at much smaller orbital radii than for stars like our Sun. Hence, characterizing the host stars of exoplanets is vital to the main goals of the *Kepler* mission. As motivated in the previous section, asteroseismology presents an ideal tool to help characterize stars in the *Kepler* field, and the common requirement for continuous, high-precision photometry has fueled a synergy between both fields which has been ideally realized within the *Kepler* project. The Kepler Asteroseismic Science Consortium (KASC, Gilliland et al. 2010a) carries out the analysis of *Kepler* time series to study variable stars, ranging from eclipsing binaries and classical pulsators, to solar-like oscillations in stars from the main-sequence to the red giant branch.